Conclusion: Cardiac involvement in $CXMD_J$ dogs is milder and has slower progression than that described in GRMD dogs. The distinct deep Q-waves have been ascribed to myocardial fibrosis in the posterobasal region of the left ventricle, but our data showed that they precede the lesion on echocardiogram and histopathology. These findings imply that studies of $CXMD_J$ may reveal not only another causative mechanism of the deep Q-waves but also more information on the pathogenesis in the dystrophin-deficient heart.

Background

Duchenne muscular dystrophy (DMD) is a common and lethal genetic disease characterized by progressive muscle wasting. It is an X-linked recessive disorder caused by mutations in the dystrophin gene, which encodes a cytoskeletal protein, dystrophin [1]. The absence of dystrophin is accompanied by a loss of dystrophin-glycoprotein complex at the sarcolemma and results in progressive degeneration of skeletal and cardiac muscle with fibrotic tissue replacement and fatty infiltration [2,3]. The onset of the disease occurs between 2 and 5 years of age, and most patients die of respiratory or cardiac failure [4,5]. Cardiac involvement, which occurs commonly in DMD patients, has increasingly become an important cause of death because recent clinical progress has reduced the risk of death due to respiratory failure [6,7].

Like dystrophin-deficient skeletal muscle, dystrophin-deficient cardiac muscle is replaced by fibrotic or fatty tissue, especially in the left ventricular posterobasal wall region [8-11]. Atrophic changes with loss of striation, vacuolation, fragmentation, or nuclear degeneration in the myocardium have also been reported [12]. Progressive involvement of the left ventricle leads to wall motion abnormality and results in dilated cardiomyopathy. In DMD patients, the electrocardiogram (ECG) may show tall R-waves in the right precordial leads, deep Q-waves in leads I, aVL, V5-6 or II, III, and aVF [8-13], as well as an increased heart rate, shortened PQ (PR) interval, conduction abnormalities or arrhythmias such as sinus arrhythmia, atrial ectopic beats, and ventricular premature complexes in DMD patients [13-16]. One of the electrocardiographic abnormalities, deep Q-waves, has been considered to be attributable to myocardial fibrosis [8,9,17]. Echocardiography indicates myocardial thickening, wall motion abnormalities, enlargement of the left ventricle, and left ventricular systolic and diastolic dysfunction. Hypokinesis of the posterobasal wall is consistent with the spreading fibrosis and significant decrease in the internal dimensions of the ventricles [14,15]. There are, however, many unresolved issues in cardiac involvement, such as the reason why the posterobasilar segment of the left ventricle is consistently the first lesion, whether extensive fibrosis involves the conduction system, the pathogenesis of inappropriate tachycardia or electrocardiographic abnormalities, and whether abnormal smooth muscle regulation affects the cardiomyopathy [18]. One way to clarify these problems is to study suitable animal models.

To date, the X-linked muscular dystrophy (*mdx*) mouse and the Golden retriever-based muscular dystrophy dog (GRMD) have been used for elucidation of the pathogenesis and development of therapy for DMD. The phenotypes of GRMD are more similar to DMD than that of the *mdx* mouse [19-21], and GRMD also shows similar electrocardiographic findings and progressive cardiomyopathy comparable to the cardiac involvement of DMD patients [20-23]. In this respect, GRMD is a useful model to explore cardiac involvement, but GRMD is very difficult to maintain because of their severe phenotypes. Mild phenotypes can be expected in small sized dogs such as Beagle, indicated by the cross-bred study by Valentine *et al.* [20]. Moreover, medium-sized Beagle is easy to handle or raise than GRMD, therefore they have definite advantages in animal housing or welfare. Therefore, we established a Beagle-based dog colony named canine X-linked muscular dystrophy in Japan ($CXMD_J$) [24]. In $CXMD_J$, involvement of the temporalis and limb muscles is observed from 2 months of age, and macroglossia, dysphagia, drooling, and joint contracture are apparent from 4 months of age; the phenotypes of $CXMD_J$ are thus almost comparable to GRMD [25]. In this study, we investigated the cardiac phenotypes in $CXMD_J$ using electrocardiography, echocardiography, and pathological examinations. Abnormalities on echocardiogram and cardiac pathology were detected from 12 months of age; however, the distinct deep Q-waves in leads II, III, and aVF on ECG were consistently observed by 6–7 months of age in all $CXMD_J$ dogs examined. The cardiac phenotypes of $CXMD_J$ were identical to but milder than those of GRMD described in the literature. Thus, $CXMD_J$ may also be a suitable animal model for elucidation of the above-mentioned problems.

Methods

Animals

We imported frozen GRMD semen and artificially inseminated a Beagle bitch. The carriers produced were mated with unrelated Beagles, and a Beagle-based canine X-linked muscular dystrophy ($CXMD_J$) breeding colony was established [24]. In this study, four normal male and eight affected male dogs of the third generation (G3) between 2 to 21 months of age were examined. All of the affected and normal dogs were descendents of a single affected

male, and were part of the $CXMD_J$ breeding colony at the General Animal Research Facility, National Institute of Neuroscience, National Center of Neurology and Psychiatry (NCNP) (Tokyo, Japan) or the Chugai Research Institute for Medical Science, Inc. (Nagano, Japan). The clinical and histopathological characteristics, except for cardiac involvement, of $CXMD_J$ dogs were recently described [25]. These dogs were cared for and treated in accordance with the guidelines provided by the Ethics Committee for the Treatment of Laboratory Middle-Sized Animals of the National Institute of Neuroscience, NCNP (Tokyo, Japan) or the Ethics Committee for Treatment of Laboratory Animal of Chugai Pharmaceutical Co., Ltd. (Tokyo, Japan). These studies were also approved by the Ethics Committee for the Treatment of Laboratory Middle-Sized Animals of NCNP (approved No. 13-03, 14-03, 15-03, 16-03, 17-03, and 18-03). All experiments were performed with consideration for preventing unnecessary pain.

Genotyping of $CXMD_J$ allele

Each affected or normal male dog was identified by genotyping. A snapback method of single-strand conformation polymorphism analysis was used to determine the GRMD allele as described previously [26].

Measurement of serum creatine kinase (CK)

Blood samples were obtained from the cephalic vein at sacrifice. Serum CK level was measured by colorimetric assay using a FDC3500 clinical biochemistry analyzer (FujiFilm Medical Co., Tokyo, Japan).

Electrocardiographic studies

Leads I, II, III, aVR, aVL and aVF were recorded in the right lateral recumbency using an ECG-922 electrocardiograph (Nihon Koden, Tokyo, Japan) [27]. All ECGs were obtained at a paper speed of 50 mm/sec and calibration of 10 mm/mV. First, the electrocardiography were performed in two $CXMD_J$ (III-302MA, III-303MA) and one normal littermate (III-301MN) dogs at 2, 3, 4, 6, 9, 12, 15, 18, and 21 months of age, and the heart rate (HR), intervals of PQ and QRS, and Q/R ratios were measured. However, in normal control and in $CXMD_J$, Q waves were not prominent in leads aVR and aVL, therefore, we measured the Q/R ratios in leads I, II, III and aVF. Next, we compared the HR, intervals of PQ and QRS, or Q/R ratios in I, II, III and aVF in eight $CXMD_J$ and four normal dogs at 6–7 months of age.

Echocardiographic studies

M-mode and two-dimensional echocardiography was performed using an EUB-8000 echocardiograph (Hitachi Medical Corporation, Tokyo, Japan). The thickness of the interventricular septum (IVS) and left ventricular posterior wall (LVPW) at end-diastole, left ventricular internal dimension at end-diastole (LVIDd) and systole (LVIDs), and fractional shortening (FS) were examined on normal and $CXMD_J$ dogs using M-mode echocardiography. We calculated the M-mode parameters based on multiple measurements of 5 consecutive heart cycles, or 3 or 5 representative heart cycles. We examined the parameters mentioned above and myocardial echogenicity in two $CXMD_J$ (III-302MA, III-303MA) and one normal littermate (III-301MN) dogs at 2, 3, 4, 6, 9, 12, 15, 18, and 21 months of age. We also examined the parameters mentioned above and myocardial echogenicity in six $CXMD_J$ (III-D53MA, III-D55MA, III-1803MA, III-D38MA, III-D02MA, III-D08MA) and three normal dogs (III-D56MN, III-1804MN, III-D03MN) at the time point just before euthanasia. Among those dogs, myocardial echogenicity in one $CXMD_J$ (III-D02MA) and its normal littermate (III-D03MN), and another $CXMD_J$ (III-D08MA) dogs were also examined at various time points.

Macroscopic and histopathological analyses

All dogs in this study underwent cardiac histological analysis. After a dog was given an overdose of intravenous pentobarbital, the whole heart was removed and immediately fixed in 15% buffered formalin. Formalin-fixed hearts were cross-sectioned, and samples were taken from the right and left ventricles at the apical papillary muscle and basal levels (each level containing the interventricular septum, anterior wall, lateral wall, and posterior wall). The tissue blocks were embedded in paraffin, and 10 μm sections were stained with hematoxylin and eosin or Masson's trichrome stain. Photographs were taken with a DAS Mikroskop LEITZ DMRB microscope (Leica, Wetzlar, Germany), using a digital still camera system HC-2500 (FujiFilm, Tokyo, Japan).

Statistics

Data are expressed as means +/- SE. Student's t test was used to evaluate differences between the two groups. A p value of less than 0.05 was considered to indicate statistical significance.

Results

Clinical profiles of $CXMD_J$

We recently reported the detailed clinical and histopathological characteristics of $CXMD_J$ except for cardiac phenotypes [25]. None of the dogs in the present study showed clinical signs of heart failure, and no murmur was present on auscultation in any $CXMD_J$ dog examined. We evaluated body and heart weight, the ratio of heart to body weight, and serum CK in eight $CXMD_J$ and four normal male dogs aged 6–21 months just before euthanasia (Table 1). There were no differences in body and heart weight and heart/body weight ratio between normal and $CXMD_J$ dogs. Serum CK levels in the $CXMD_J$ dogs ranged from 12,500 to 13 8,000 IU/1. These values were signifi-

cantly different from those in normal control dogs (60 to 515 IU/1). One 9-month-old $CXMD_J$ dog, III-D55MA, did not show any signs of respiratory or cardiac failure. When we tried to record a routine ECG of the dog, the dog struggled to escape from recording and then ceased moving. Immediately afterwards, we recorded ECG and the monitor showed an idioventricular rhythm. The dog died despite attempted cardiopulmonary resuscitation.

Electrocardiographic findings

The HR and PQ intervals of the affected littermates were no different from those recorded from a normal littermate at 12 months of age, but we detected an increase in HR and a decrease in PQ interval in the affected dogs after 15 months of age (Fig. 1A). The HR and PQ intervals were negatively correlated both in normal and affected dogs (data not shown). The QRS interval in the affected dogs did not differ from that in the normal littermate at any age (Fig. 1A). Prominent deep Q-waves were observed in limb leads II, III, and aVF in some $CXMD_J$ dogs, but not in the normal littermates, as shown in Fig. 1B. The Q/R ratios were definitely increased in the affected littermates at 6 months of age or older compared with the normal littermate (Fig. 1C). In all normal and $CXMD_J$ dogs at 6–7 months of age, the HR, and intervals of PQ and QRS were not different between the two groups of dogs (Fig. 2A), but the Q/R ratios in leads II, III, and aVF in the affected dogs were significantly higher than those in the normal dogs (Fig. 2B).

Echocardiographic findings

The thickness of LVIDd, IVS, and PW in two $CXMD_J$ (III-302MA, III-303MA) were not different from those in a normal littermate (III-301MN) by sequential analysis with advancing age (Fig. 3A). Those parameters were not different between other six $CXMD_J$ and three normal dogs, when examined just before euthanasia (Table 2). FS in III-302MA decreased with advancing age, and the value (27.3%) at 21 months of age was lower than that of the normal littermate, but was within normal range reported previously [28,29]. FS in the other seven $CXMD_J$ were normal, even just before euthanasia (Table 2). A mild hypokinesis of the left ventricular wall was detected in III-302MA at 21 months of age (Fig. 3B), but any clinical signs had not been developed in the dog.

The sequential studies of myocardial echogenicity with advancing age in III-302MA and in III-303MA demonstrated that the hyperechoic lesions in the left ventricular posterior wall were seen at 12 months of age or older (Fig. 4A, Table 3). In the subsequent examinations of six $CXMD_J$, we found the hyperechoic lesion in a $CXMD_J$, III-D08MA, at 5 months of age (Fig. 4B, Table 3), however the hyperechoic lesion was not detected in other four $CXMD_J$ at 5 to 7 months old (Fig. 4B, Table 3). One $CXMD_J$, III-D38MA, did not reveal any hyperechoic lesions when examined at 12 months of age, but has not been examined at 5 to 7 months of age (Table 3). Taken these echocardiographic data, it is considered that the cardiac functions in $CXMD_J$ were basically maintained well by 21 months of age, despite showing hyperechoic lesions of the left ventricle in limited numbers of $CXMD_J$.

Macroscopic and histopathological findings

The right and left ventricular walls were examined macroscopically and histopathologically in four normal and eight affected male dogs at the ages shown in Table 1. The base view of the formalin-fixed heart did not show any macroscopic lesions in III-1803MA at 7 months and III-302MA at 21 months of age (Fig. 5A) like other affected dogs (data not shown). No histopathological abnormality was found in the posterior wall of the left ventricle of

Table 1: Clinical profiles of normal and $CXMD_J$ male dogs

	Age (mo)	BW(g)	HW(g)	HW/BW (%)	Serum CK (IU/l)
Normal dogs					
III-D56MN	6	12.0	95.1	0.97	515
III-1804MN	7	13.6	110.0	0.81	215
III-D03MN	14	13.1	127.0	0.84	215
III-301 MN	21	14.4	120.0	0.96	60
$CXMD_J$ dogs					
III-D53MA	6	9.6	91.9	0.90	63,100
III-D55MA	7	10.0	80.0	0.80	42,000
III-1803MA	9	14.4	128.6	0.69	69,100
III-D38MA	12	11.4	78.8	1.01	138,000
III-D02MA	15	9.1	92.0	0.87	17,600
III-D08MA	15	12.0	104.3	0.97	40,700
III-302MA	21	12.4	120.0	0.86	12,500
III-303MA	21	13.9	120.0	0.80	23,000

BW, body weight; HW, heart weight; HW/BW, heart weight/body weight ratio; * $p < 0.01$ normal dogs *vs* $CXMD_J$ dogs

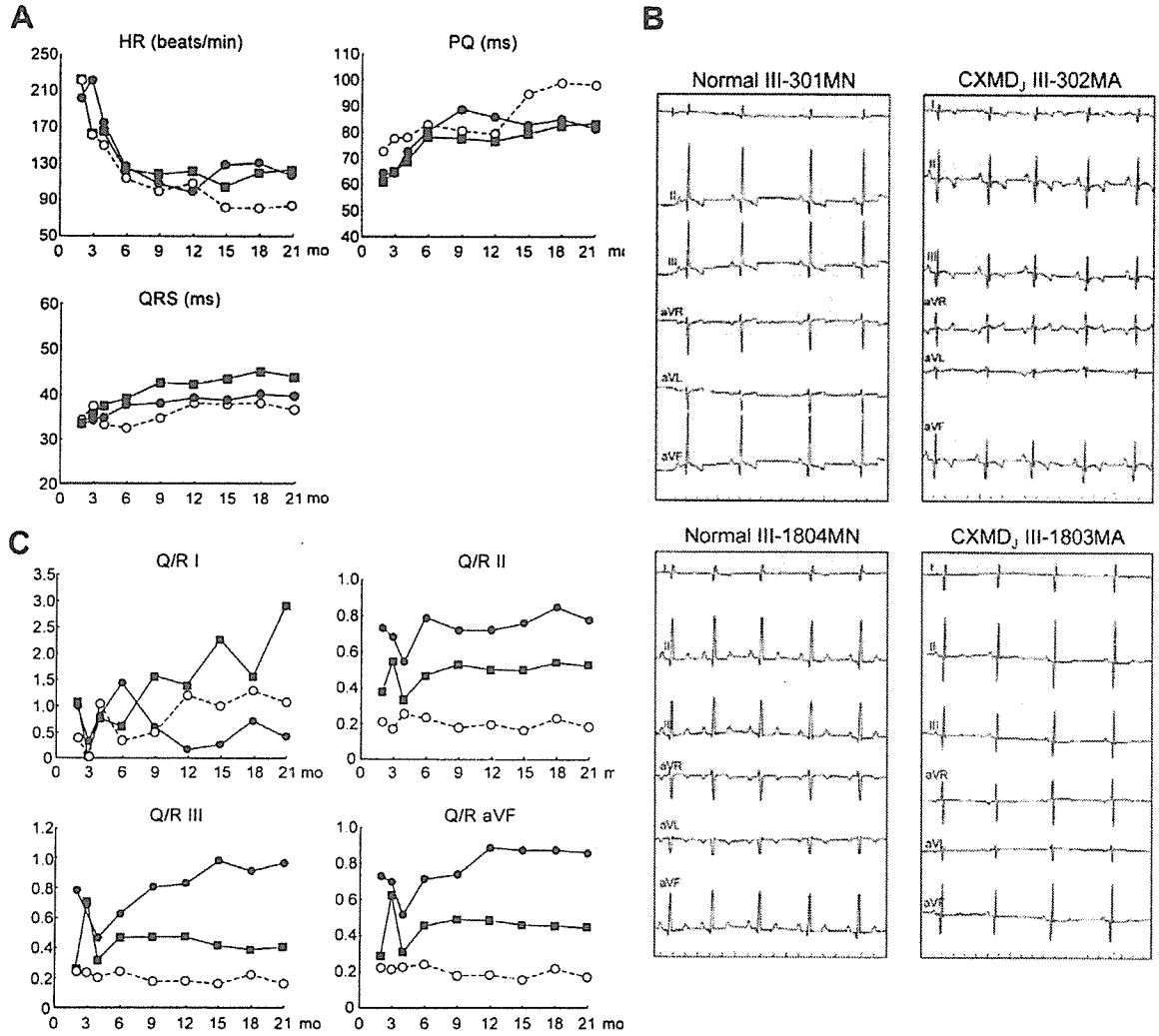

Figure 1

Electrocardiographic findings in CXMD$_J$ A: Sequential studies in electrocardiographic parameters with advancing age in normal and CXMD$_J$ dogs. Heart rate (HR) (beats/min), PQ interval (ms), and duration (ms) of QRS complex on ECG in a normal littermate III-301MN (open circle), and CXMD$_J$ dogs III-302MA (closed circle) and III-303MA (closed square) at 2, 3, 4, 6, 9, 12, 15, 18, and 21 months of age. **B**: Representative ECGs in normal and CXMD$_J$ male dogs. ECGs were recorded from normal dogs, III-301MN and III-1804MN, and CXMD$_J$ dogs, III-302MA and III-1803MA, at 6 months of age. Distinct deep Q waves were present in the CXMD$_J$ dogs. Leads were recorded at 50 mm/s, 1 cm/mV. **C**: Sequential studies in Q/R ratios with advancing age in limb leads I, II, III, and aVF in normal and CXMD$_J$ dogs. Q/R ratios in limb leads I, II, III, and aVF in a normal littermate III-301MN (open circle), and the CXMD$_J$ dogs III-302MA (closed circle) and III-303MA (closed square) at 2, 3, 4, 6, 9, 12, 15, 18, and 21 months of age.

affected dogs III-1803MA, III-D55MA, and III-D02MA (Fig. 5B), and other affected dogs under the age of 12 months (III-D53MA, III-D38MA). On the other hand, moderate fibrosis in the left ventricular wall, especially on the posterior side, was detected in an affected dog, III-302MA, at 21 months (Fig. 5B) as well as in III-D08MA at

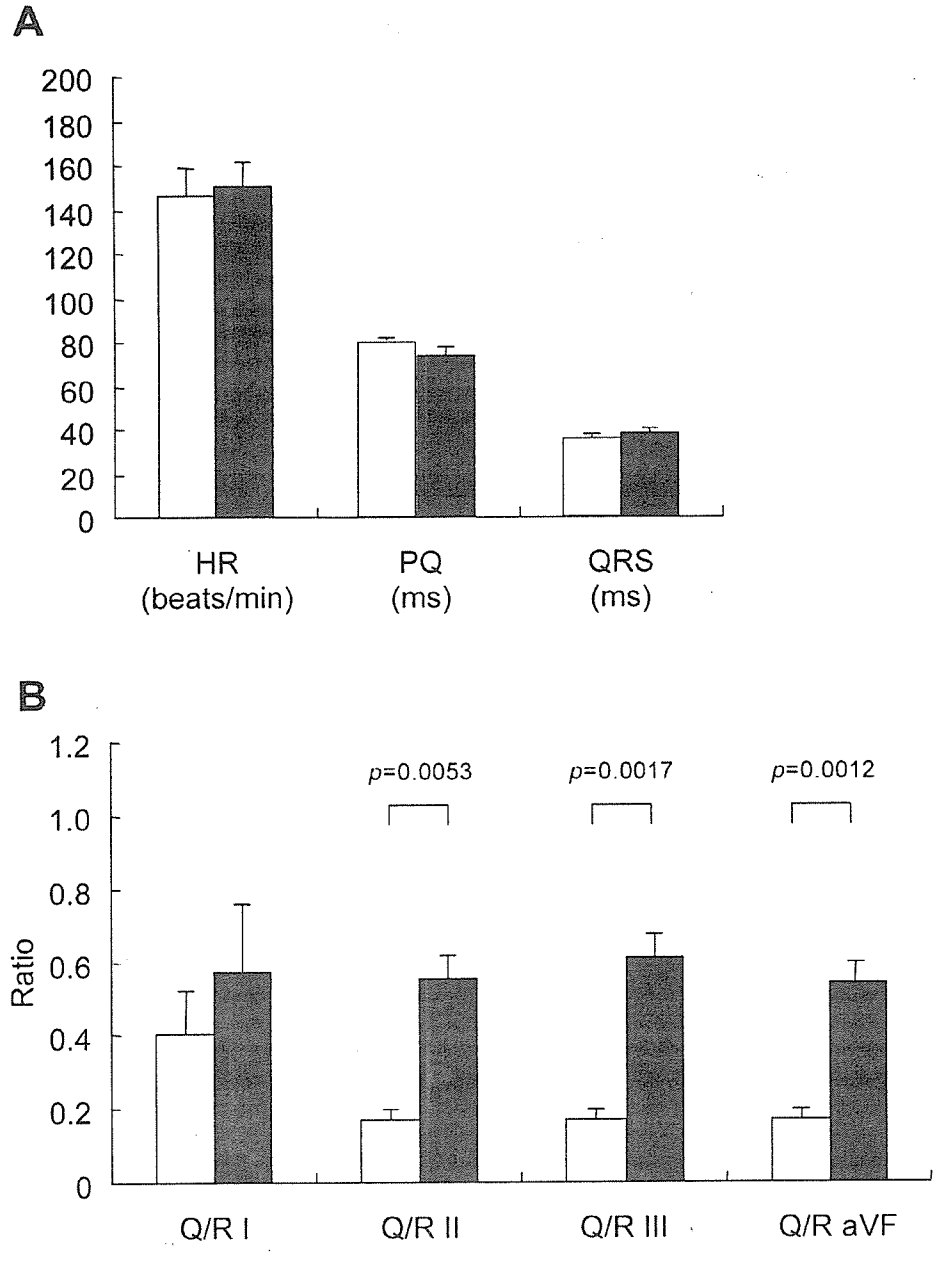

Figure 2
Comparison of electrocardiographic parameters and Q/R ratios between normal and $CXMD_J$ dogs at 6–7 months of age A. Heart rate (HR) (beats/min), PQ interval (ms), and duration of QRS complex (ms) on ECG in normal (n = 4) and $CXMD_J$ (n = 8) dogs at 6–7 months of age. White columns indicate normal dogs, and black columns represent $CXMD_J$ dogs. Bar shows mean +/- SE. **B.** Q/R ratios in limb leads I (Q/R I), II (Q/R II), III (Q/R III), and aVF (Q/R aVF) on ECG in normal (n = 4) and $CXMD_J$ (n = 8) dogs at 6–7 months of age. White columns indicate normal dogs, and black columns represent $CXMD_J$ dogs. Bar shows mean +/- SE.

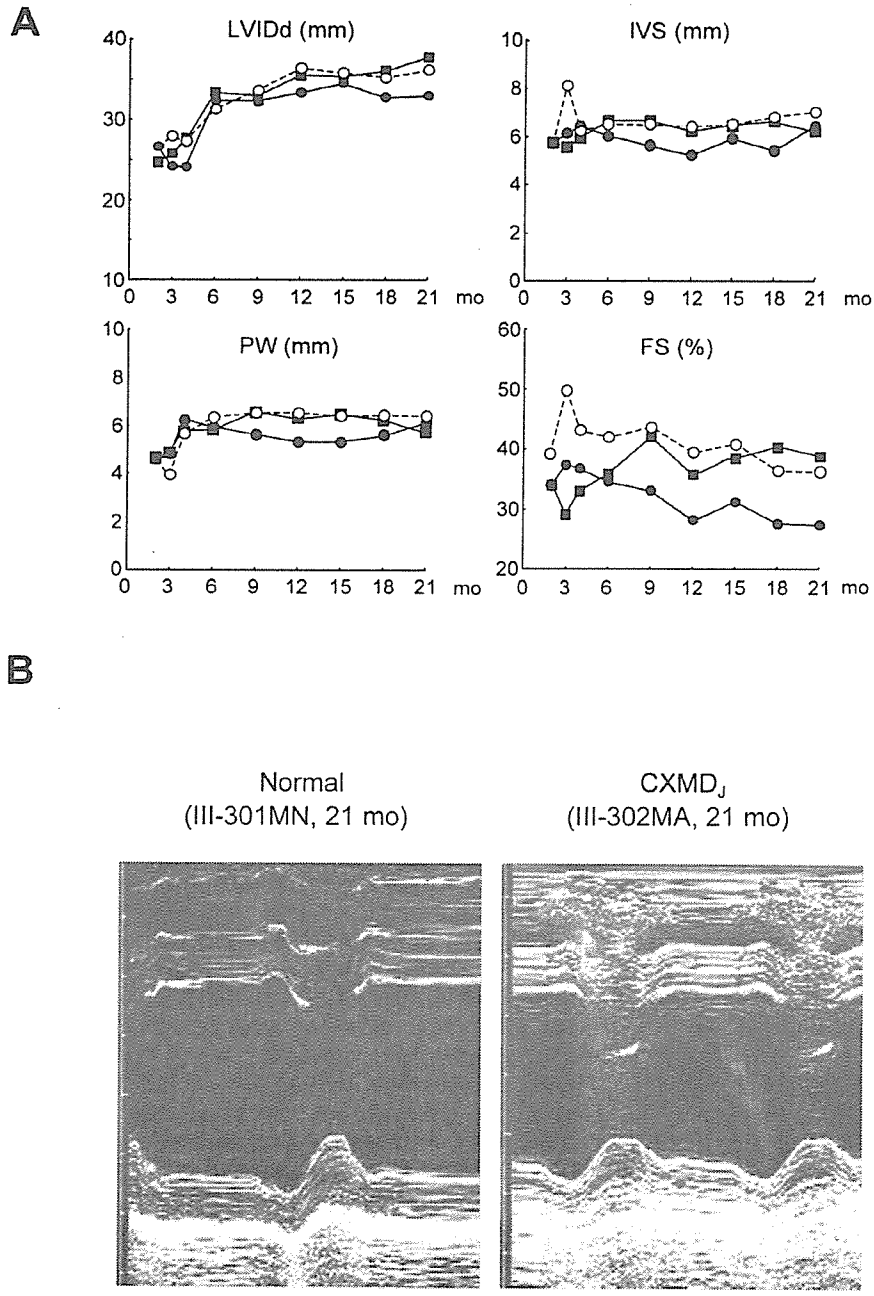

Figure 3
Cardiac function by echocardiography in CXMD$_J$ A: Sequential studies in echocardiographic parameters with advancing age in normal and CXMD$_J$ dogs. LVIDd (mm), IVS and PW thickness (mm), and FS (%) in a normal littermate III-301MN (open circle), and the CXMD$_J$ dogs III-302MA (closed circle) and III-303MA (closed square) at 2, 3, 4, 6, 9, 12, 15, 18, and 21 months of age. **B**: M-mode echocardiogram in a normal littermate III-301MN, compared to the CXMD$_J$ dog III-302MA at 21 months of age. Hypokinesis of the left ventricular posterior wall was observed in the CXMD$_J$ dog.

Table 2: Echocardiographic findings in normal and $CXMD_J$ male dogs

	Age (mo)	LVIDd (mm)	LVIDs (mm)	IVS (mm)	PW (mm)	FS (%)
Normal male dogs						
III-D56MN	6	34.2	12.5	6.6	5.6	63.5
III-1804MN	7	30.7	18.9	8.2	7.4	38.4
III-D03MN	14	32.8	16.8	10.0	9.4	48.7
III-301 MN	21	36.1	23.0	7.0	6.4	36.2
$CXMD_J$ male dogs						
III-D53MA	6	29.7	19.7	8.0	7.2	33.8
III-D55MA	7	28.7	15.4	6.3	6.3	46.5
III-1803MA	7	32.5	16.7	5.8	7.5	48.5
III-D38MA	12	30.3	18.8	8.4	5.8	37.8
III-D02MA	15	27.5	17.3	9.1	8.8	37.0
III-D08MA	15	39.5	24.9	5.9	5.9	36.9
III-302MA	21	32.9	23.9	6.4	6.1	27.3
III-303MA	21	37.6	23.1	6.2	5.7	38.6

Age, age at examination; LVIDd, LV internal dimension diastolic; LVIDs, LV internal dimension systolic; IVS, intraventricular septum thickness; PW, posterior wall thickness; FS, fractional shortening

15 months and III-303MA at 21 months of age (data not shown). We found that the right ventricular walls were kept intact in all $CXMD_J$ dogs examined.

Discussion

In electrocardiographic findings, an increased HR and a shortened PQ interval have been reported in both DMD patients [13] and GRMD [22]. These findings were also observed in $CXMD_J$ dogs. Increased sympathetic activity and decreased parasympathetic activity have been observed in DMD patients and are associated with disease progression [30]; therefore, autonomic dysfunction in dystrophin deficiency might affect these parameters. It has been reported that HR is negatively correlated with PQ interval in normal Beagle dogs and it may be ascribed to a parasympathetic input at the level of the AV node [31]. The negative correlation between HR and PQ intervals was also found in affected dogs, indicating the parasympathetic input was maintained well even in affected dogs at AV node level. The QRS duration was within normal limits in the $CXMD_J$ dogs, which is compatible with most cases of DMD [13]. Another peculiar electrocardiographic finding in DMD is the deep and narrow Q-waves in I, aVL and V6 or in II, III and aVF [10,13,16,32]. $CXMD_J$ dogs also showed prominent Q-waves and increases in the Q/R ratio in leads II, III, and aVF, findings that are consistent with those in GRMD [23]. In all $CXMD_J$ dogs examined, the distinct deep Q-waves were recognized by 6–7 months of age, which is earlier than the other abnormal electrocardiographic parameters, and the Q/R ratio in affected dogs remained high from 6 to 21 months of age. Actually, the prominent Q-wave and increase in Q/R ratio were also detected in some of the $CXMD_J$ dogs at around 2 months of age (Fig. 1C), but it is difficult to evaluate the degree of the Q/R ratio increase before 3 months of age because the QRS vector is almost exclusively directed to the right and varies significantly in the weeks after birth [33]. A previous report described GRMD dogs ranging from 6 months to > 2 years as having deep Q-waves and increased Q/R ratios in leads II, III, and aVF [23]. The Q-waves, however, might have been seen earlier and regarded as normal variants or not have been considered important for the reasons mentioned above.

Hyperechoic lesions indicating myocardial fibrosis in the posterobasal left ventricular wall have been detected by echocardiography in GRMD dogs as well as DMD patients [22,23]. Moise *et al.* reported that hyperechoic lesions were first detected in eight of eleven GRMD dogs (73%) by 6–7 months of age and that they correlated with histologically recognizable areas of mineralization and corresponded to the progression of fibrosis [23]. In our study, one of eight of $CXMD_J$ dogs showed a hyperechoic lesion in the left ventricular posterior wall, but the rest had not by the age of 6–7 months (Table 3, Fig. 4). The hyperechoic lesion in the left ventricular posterior walls was detected in both III-302MA and III-303MA, but not early as 12 months of age (Table 3). The results of echocardiography indicated that the cardiac involvement in $CXMD_J$ is milder than that in GRMD. Echocardiography did not reveal particular left ventricular dysfunction in any $CXMD_J$ dog by 21 months of age, but a mild hypokinesis of the left ventricular wall was observed in III-302MA at 21 months of age (Fig. 3B). The dysfunction found in the dog, however, was mild and the dog had no cardiac symptom. Moise *et al.* reported that three of the six GRMD dogs > 2 years of age showed a decrease in fractional shortening, but did not mention at what age the abnormal cardiac findings appeared.

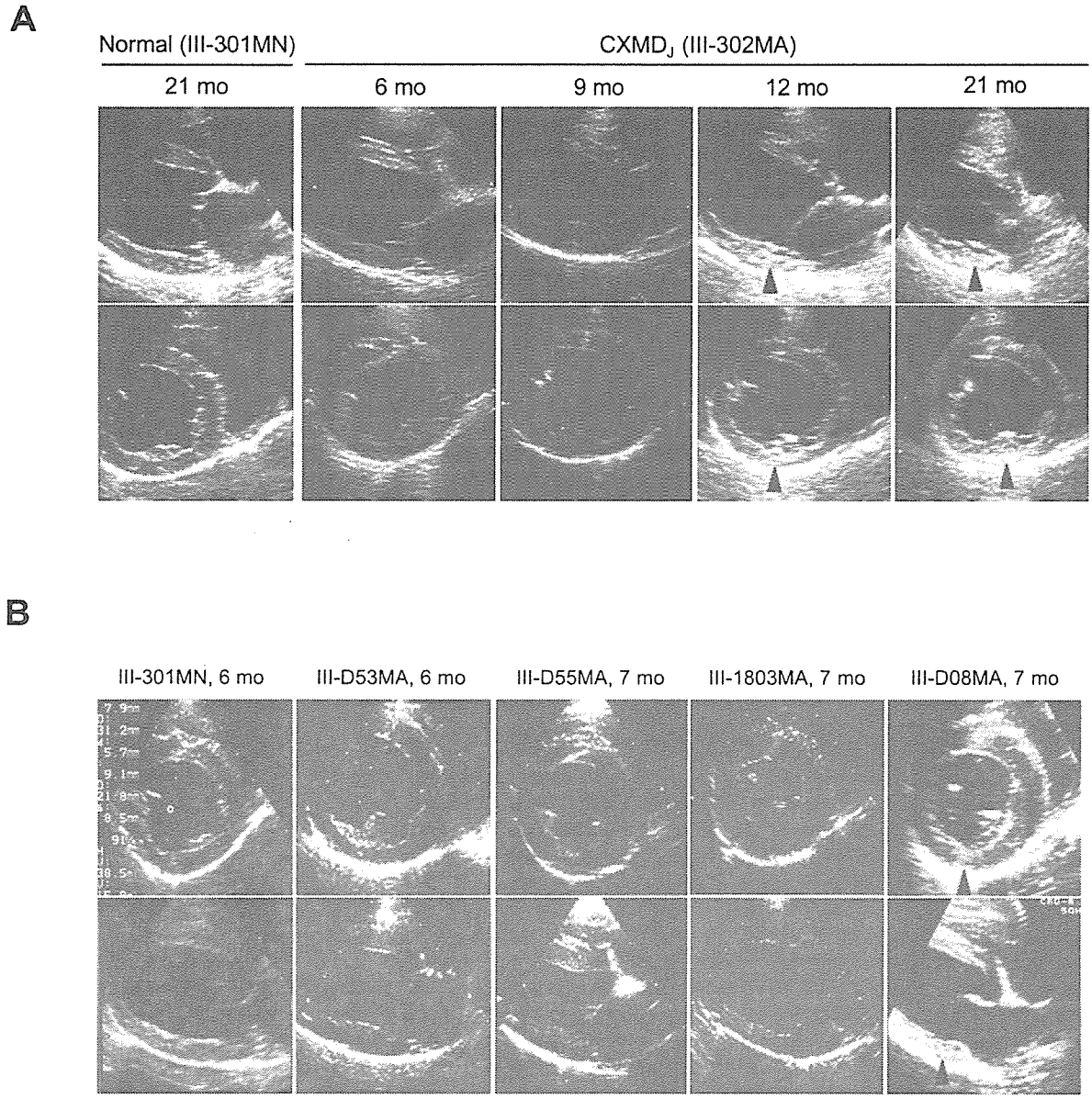

Figure 4
Echogenicity in CXMD$_J$ A: Sequential studies in echogenicity with advancing age by two-dimensional echocardiography in a normal dog III-301MN, and a CXMD$_J$ dog III-302MA, at 6–21 months of age. Hyperechoic lesions (arrowheads) of the left ventricular posterior wall were detected in the CXMD$_J$ dog at 12 months of age and older.**B**: Two-dimensional echocardiograms of a normal dog III-301MN at 6 months of age, and four CXMD$_J$ dogs III-D53MA, III-D55MA, III-1803MA, and III-D08MA at 6 to 7 months of age. The hyperechoic lesion (arrowhead) was detected only in the left ventricular posterior wall of III-D08MA.

Previous studies of morphology in GRMD showed that myocardial involvement is initially found in the left posterobasal ventricular wall, similar to that of patients with DMD [21-23]. Valentine *et al.* reported that GRMD dogs

Table 3: Echogenicity of left ventricular posterior wall in normal and CXMD$_J$ male dogs

	Months of age (mo)																			
	2	3	4	5	6	7	8	9	10	11	12	13	14	15	16	17	18	19	20	21
Normal dogs																				
III-D56MN					(-)*															
III-1804MN					(-)	(-)*														
III-D03MN	(-)			(-)		(-)			(-)			(-)	(-)*							
III-301 MN	(-)	(-)	(-)		(-)			(-)			(-)			(-)			(-)			(-)*
CXMD$_J$ dogs																				
III-D53MA					(-)*															
III-D55MA						(-)		*												
III-1803MA					(-)	(-)*														
III-D38MA											(-)*									
III-D02MA	(-)			(-)		(-)					(-)	(-)		(-)*						
III-D08MA	(-)			(+)		(+)					(+)	(+)		(+)*						
III-302MA	(-)	(-)	(-)		(-)			(-)			(+)			(+)			(+)			(+)*
III-303MA	(-)	(-)	(-)		(-)			(-)			(+)			(+)			(+)			(+)*

Hyperechoic lesion +, positive; -, negative; Asterisk in each CXMD$_J$ dog shows age at euthanasia.

at 6.5 months of age had acute severe lesions with focal myocardial mineralization associated macrophages and giant cells in the left ventricular papillary muscle and left ventricular wall [22]. Moreover, GRMD dogs at 12 months of age or older demonstrated prominent myocardial fibrosis in more widespread lesions [22]. The myocardial fibrosis of the left ventricular wall in the older stage of CXMD$_J$ dogs was consistent with that in DMD patients and GRMD dogs. The change was detected at 15 months of age or older in the CXMD$_J$ (III-D08MA, III-302MA, and III-303MA), although III-D08MA showed a hyperechoic lesion at 5 months of age or older (Table 3). The cardiac involvement in CXMD$_J$, therefore, was milder and slowly progressed than that in GRMD, although a longer period evaluation of large numbers of CXMD$_J$ will be needed to conclude the mild cardiac phenotypes of CXMD$_J$.

Why is the cardiac involvement in CXMD$_J$ milder than that in GRMD? Valentine *et al.* reported that skeletal muscle involvement in small dystrophic dogs was milder than that in large ones [19]. Several reports on dystrophic features have hypothesized that the clinical severity may be associated with growth rate [34] or muscle fiber diameter [35]. Living in a cage rather than running free could also affect the cardiac phenotypes of CXMD$_J$ because physical exercise promotes cardiac involvement in dystrophin-deficient *mdx* mice [36]. The difference in the genetic background between GRMD, golden retriever and CXMD$_J$, Beagle might also affect the disease progression.

The prominent deep Q-waves seen in both DMD and GRMD have been attributed to a reduction in or a loss of electromotive force caused by scarring of the posterobasal region of the left ventricle [8,9,17]. In our study, the deep Q-waves and increases in the Q/R ratio in CXMD$_J$ preceded the lesions seen on echocardiogram and histopathology, as shown in Fig. 6. Considering this result, the origin of the distinctive Q-waves might not be associated with the myocardial lesion in the posterobasal left ventricular wall. It has recently been reported that expression of a transgene in *mdx* mice for neuronal nitric oxide synthase (nNOS), which occurs as a secondary loss in dystrophin deficiency, decreased cardiac inflammation and fibrosis resulting in amelioration of both cardiac function and electrocardiographic abnormalities, including deep Q-waves [37]. Perloff *et al.* suggested that the alteration of a particular ionic current by lack of specific membrane proteins associated with dystrophin might participate in electrocardiographic changes [17]. We will not therefore deny that minimal myocardial damage could be associated with the pathogenesis of deep Q-waves, but our results suggest that an investigation of the conduction and cardiovascular systems will also be needed to explore the pathophysiology of the deep Q-waves in dystrophin-deficient heart. In this regard, CXMD$_J$ will be very useful to elucidate aspects of the dystrophin-deficient heart, but we may recognize that a longer period of time would be required to complete cardiac phenotypes in CXMD$_J$.

Conclusion

We demonstrated that the cardiac phenotypes of CXMD$_J$ are comparable to but milder than those of GRMD. Furthermore, we found for the first time that the distinct deep Q-waves precede detection of the left ventricular posterobasal lesion by echocardiography or histopathology. CXMD$_J$ may provide not only new insights into the mech-

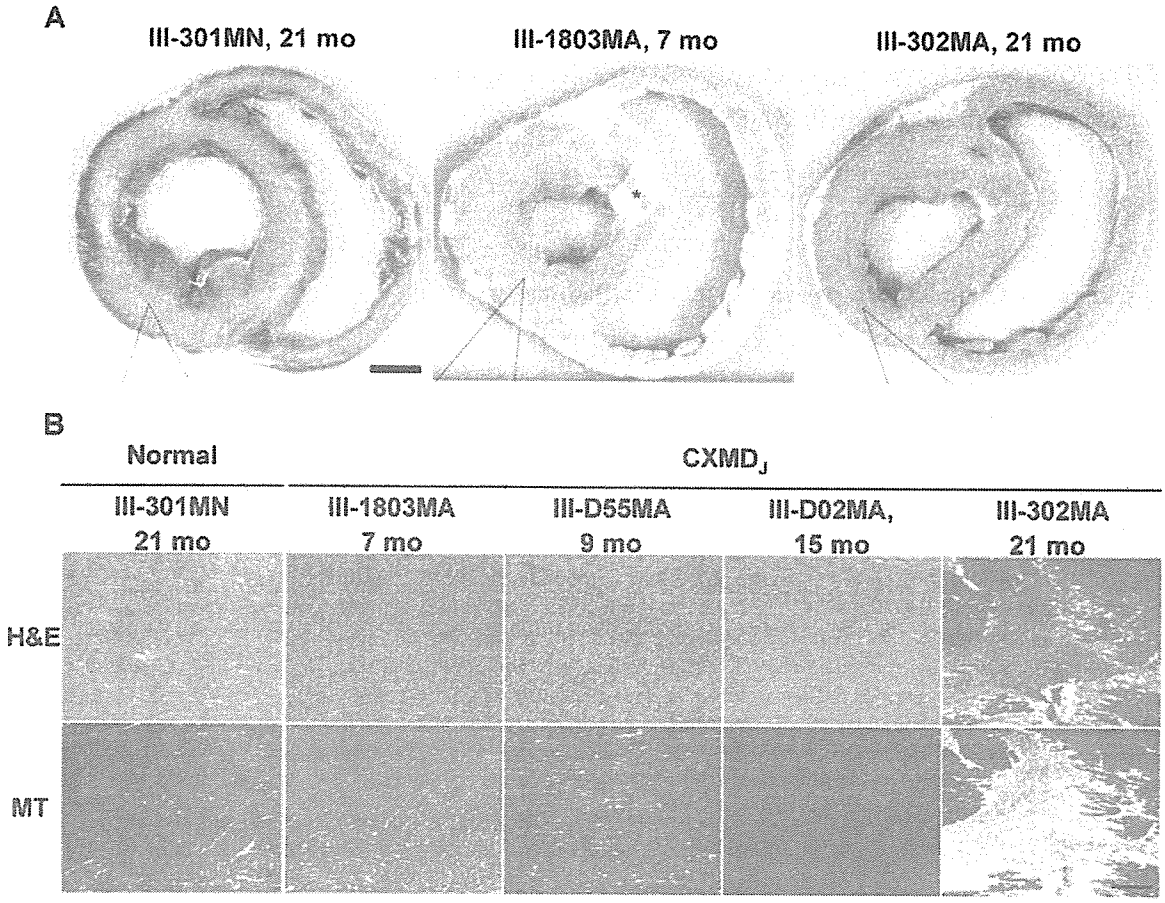

Figure 5
Macroscopic and histopathological findings in CXMD$_J$ hearts A. Macroscopic examinations of the base of the formalin-fixed hearts of a normal littermate III-301MN at 21 months and CXMD$_J$ dogs, III-1803MA at 7 months and III-302MA at 21 months of age. *Aortic valve. Bar shows 1 cm. **B.** Hematoxylin and eosin (H&E) and Masson's trichrome (MT) staining for histopathological evaluation of the left ventricular posterior wall in a normal littermate, III-301MN at 21 months and the CXMD$_J$ dogs, III-1803MA at 7 months, III-D55MA at 9 months, III-D02MA at 15 months, and III-302MA at 21 months of age. Posterior walls of left ventricles of both III-D55MA and III-D02MA were macroscopically normal (data not shown). Bar shows 200 μm.

anisms causing the abnormal Q-waves but also more information on the pathogenesis in the dystrophin-deficient heart.

Competing interests
The author(s) declare that they have no competing interests.

Authors' contributions
NY and NU carried out the electrocardiographic, echocardiographic, and pathological examination and drafted the manuscript. YF performed the electrocardiographic study. MY, KY and MRW participated in the necropsy and pathological examination. MN, YS, MT and AT participated in the maintenance of the dog colony and the design of the study. NM performed the pathological examination. YW participated in the design of the study. AN participated in the statistical analysis and drafted manuscript. ST participated in the design, planning and coordination of the study. All authors read and approved the final manuscript.

Acknowledgements

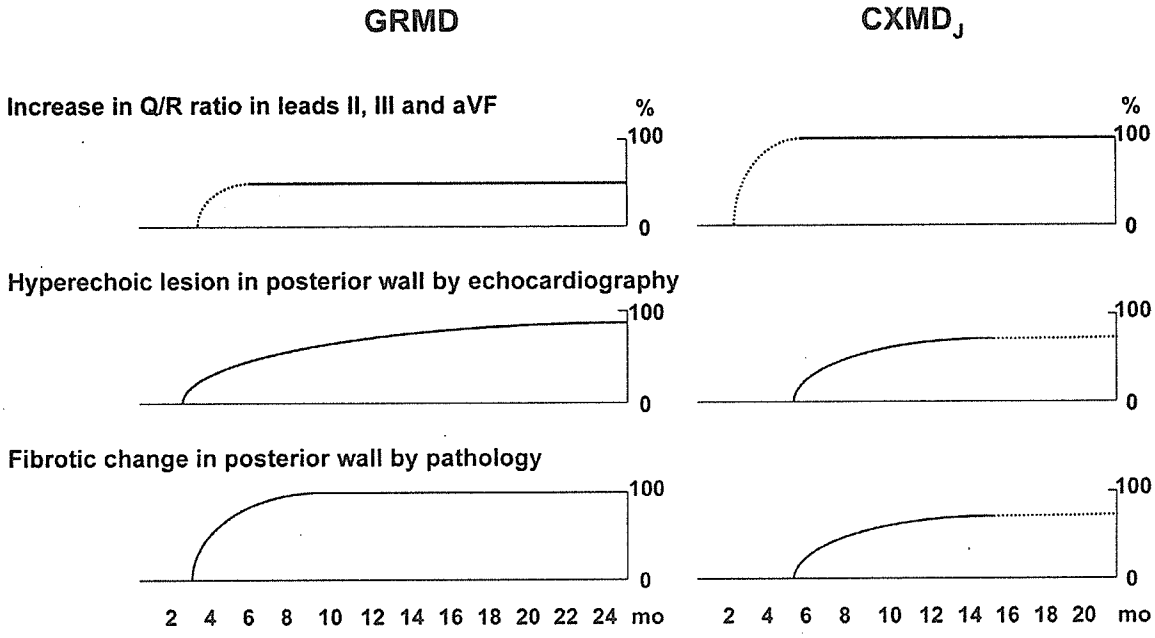

Figure 6

Comparison of cardiac involvement between GRMD and $CXMD_J$ with advancing age. Subjects were compared as follows: increase in Q/R ratio in leads II, III, and aVF in ECG, hyperechoic lesion in posterior wall by echocardiography, and fibrotic change in left ventricular posterior wall by pathology. The data on GRMD was based on the previous literature [22–24]. It is difficult to evaluate Q/R ratio in early stage of GRMD and $CXMD_J$. It is also difficult to evaluate hyperechoic lesion in echocardiogram and fibrotic change in pathology at late stage of $CXMD_J$ due to small numbers of examination ($n < 3$).

We thank Hideki Kita, Shin'ichi Ichikawa, Yumiko Yahata, and Kazue Kinoshita (JAC, Inc., Tokyo) for maintaining the dogs, Yoshikuni Tanioka (Central Institute for Experimental Animals, Kawasaki) for his support and valuable suggestions, and Ryoko Nakagawa (Department of Molecular Therapy, National Institute of Neuroscience, NCNP, Tokyo) for her technical assistance. This study was supported by Health Sciences Research Grants for Research on Psychiatric and Neurological Diseases and Mental Health (H12-kokoro-025, H15-kokoro-021, H18-kokoro-019), the Human Genome and Gene Therapy (H13-genome-001, H16-genome-003) from the Ministry of Health, Labor and Welfare of Japan, and Grants-in-Aid for Scientific Research from the Ministry of Education, Science, Sports and Culture of Japan (to S.T.).

References

1. Koenig M, Hoffman EP, Bertelson CJ, Monaco AP, Feener C, Kunkel LM: **Complete cloning of the Duchenne muscular dystrophy (DMD) cDNA and preliminary genomic organization of the *DMD* gene in normal and affected individuals.** *Cell* 1987, **50**:509-517.
2. Cullen MJ, Mastaglia FL: **Morphological changes in dystrophic muscle.** *Br Med Bull* 1980, **36**:145-152.
3. Ervasti JM, Ohlendieck K, Kahl SD, Gaver MG, Campbell KP: **Deficiency of a glycoprotein component of the dystrophin complex in dystrophic muscle.** *Nature* 1990, **345**:315-319.
4. Gilroy J, Cahalan JL, Berman R, Newman M: **Cardiac and pulmonary complications in Duchenne's progressive muscular dystrophy.** *Circulation* 1963, **27**:484-493.
5. Moser H: **Duchenne muscular dystrophy: pathogenetic aspects and genetic prevention.** *Hum Genet* 1984, **66**:17-40.
6. Mukoyama M, Kondo K, Hizawa K, Nishitani H: **Life spans of Duchenne muscular dystrophy patients in the hospital care program in Japan.** *J Neurol Sci* 1987, **81**:155-158.
7. Eagle M, Baudouin SV, Chandler C, Giddings DR, Bullock R, Bushby K: **Survival in Duchenne muscular dystrophy: improvements in life expectancy since 1967 and the impact of home nocturnal ventilation.** *Neuromuscul Disord* 2002, **12**:926-929.
8. Perloff JK, Roberts WC, de Leon AC Jr, O'Doherty D: **The distinct electrocardiogram of Duchenne's progressive muscular dystrophy. An electrocardiographic-pathologic correlative study.** *Am J Med* 1967, **42**:179-188.
9. Sanyal SK, Johnson WW, Thapar MK, Pitner SE: **An ultrastructural basis for electrocardiographic alterations associated with Duchenne's progressive muscular dystrophy.** *Circulation* 1978, **57**:1122-1129.
10. Perloff JK, de Leon AC Jr, O'Doherty D: **The cardiomyopathy of progressive muscular dystrophy.** *Circulation* 1966, **33**:625-648.
11. Frankel KA, Rosser RJ: **The pathology of the heart in progressive muscular dystrophy: epimyocardial fibrosis.** *Hum Pathol* 1976, **7**:375-386.
12. James TN: **Observation on the cardiovascular involvement, including the cardiac conduction system, in progressive muscular dystrophy.** *Am Heart J* 1962, **63**:48-56.

13. Finsterer J, Stöllberger C: **The heart in human dystrophinopathies.** *Cardiology* 2003, **99**:1-19.
14. Farah MG, Evans EB, Vignos PJ jr: **Echocardiographic evaluation of left ventricular function in Duchenne's muscular dystrophy.** *Am J Med* 1980, **69**:248-254.
15. D'Orsogna L, O'Shea JP, Miller G: **Cardiomyopathy of Duchenne muscular dystrophy.** *Pediatr Cardiol* 1988, **9**:205-213.
16. Perloff JK: **Cardiac rhythm and conduction in Duchenne's muscular dystrophy: a prospective study of 20 patients.** *J Am Coll Cardiol* 1984, **3**:1263-1268.
17. Perloff JK, Moise NS, Stevenson WG, Gilmour RF: **Cardiac electrophysiology in Duchenne muscular dystrophy: From basic science to clinical expression.** *J Cardiovasc Electrophysiol* 1992, **3**:394-409.
18. Goodwin FC, Muntoni F: **Cardiac involvement in muscular dystrophies: molecular mechanisms.** *Muscle Nerve* 2005, **32**:577-588.
19. Cooper BJ, Winand NJ, Stedman H, Valentine BA, Hoffman EP, Kunkel LM, Scott MO, Fischbeck KH, Kornegay JN, Avery RJ, Williams JR, Schmickel RD, Sylvester JE: **The homologue of the Duchenne locus is defective in X-linked muscular dystrophy of dogs.** *Nature* 1988, **334**:154-156.
20. Valentine BA, Cooper BJ, de Lahunta A, O'Quinn R, Blue JT: **Canine X-linked muscular dystrophy. An animal model of Duchenne muscular dystrophy: clinical studies.** *J Neurol Sci* 1988, **88**:69-81.
21. Valentine BA, Winand NJ, Pradhan D, Moise NS, de Lahunta A, Kornegay JN, Cooper BJ: **Canine X-linked muscular dystrophy as an animal model of Duchenne muscular dystrophy: a review.** *Am J Med Genet* 1992, **42**:352-356.
22. Valentine BA, Cummings JF, Cooper BJ: **Development of Duchenne-type cardiomyopathy. Morphologic studies in a canine model.** *Am J Pathol* 1989, **135**:671-678.
23. Moise NS, Valentine BA, Brown CA, Erb HN, Beck KA, Cooper BJ, Gilmour RF: **Duchenne's cardiomyopathy in a canine model: electrocardiographic and echocardiographic studies.** *J Am Coll Cardiol* 1991, **17**:812-820.
24. Shimatsu Y, Katagiri K, Furuta T, Nakura M, Tanioka Y, Yuasa K, Tomohiro M, Kornegay JN, Nonaka I, Takeda S: **Canine X-linked muscular dystrophy in Japan ($CXMD_J$).** *Exp Anim* 2003, **52**:93-97.
25. Shimatsu Y, Yoshimura M, Yuasa K, Urasawa N, Tomohiro M, Nakura M, Tanigawa M, Nakamura A, Takeda S: **Major clinical and histopathological characteristics of canine X-linked muscular dystrophy in Japan, $CXMD_J$.** *Acta Myol* 2005, **24**:145-154.
26. Honeyman K, Carville KS, Howell JM, Fletcher S, Wilton SD: **Development of a snapback method of single-strand conformation polymorphism analysis for genotyping Golden Retrievers for the X-linked muscular dystrophy allele.** *Am J Vet Res* 1999, **60**:734-737.
27. Tilley LP: **Basic canine and feline electrocardiography.** *Can Vet J* 1981, **22**:23-25.
28. Crippa L, Ferro E, Melloni E, Brambilla P, Cavalletti E: **Echocardiographic parameters and indices in the normal Beagle dog.** *Lab Anim* 1992, **26**:190-195.
29. Cornell CC, Kittleson MD, Della Torre P, Häggström J, Lombard CW, Pedersen HD, Vollmar A, Wey A: **Allometric scaling of M-mode cardiac measurements in normal adult dogs.** *J Vet Intern Med* 2004, **18**:311-321.
30. Yotsukura M, Fujii K, Katayama A, Tomono Y, Ando H, Sakata K, Ishihara T, Ishikawa K: **Nine-year follow-up study of heart rate variability in patients with Duchenne-type progressive muscular dystrophy.** *Am Heart J* 1998, **136**:289-296.
31. Hanton G, Rabemampianina Y: **The electrocardiogram of the beagel dog: reference values and effect of sex, genetic strain, body position and heart rate.** *Lab Anim* 2006, **40**:123-136.
32. Sanyal SK, Johnson WW: **Cardiac conduction abnormalities in children with Duchenne's progressive muscular dystrophy: electrocardiographic features and morphologic correlates.** *Circulation* 1982, **66**:853-863.
33. Trautvetter E, Detweiler DK, Patterson DF: **Evolution of the electrocardiogram in young dogs during the first 12 weeks of life.** *J Electrocardiol* 1981, **14**:267-273.
34. Zats M, Betti RT: **Benign Duchenne muscular dystrophy in a patient with growth hormone deficiency.** *Am J Med Genet* 1986, **24**:567-572.
35. Braund KG, McGuire JA, Lincoln CE: **Observations on normal skeletal muscle of mature dogs: a cytochemical, histochemical, and morphometric study.** *Vet Pathol* 1982, **19**:577-595.
36. Nakamura A, Yoshida K, Takeda S, Dohi N, Ikeda S: **Progression of dystrophic features and activation of mitogen-activated protein kinases and calcineurin by physical exercise, in hearts of mdx mice.** *FEBS Lett* 2002, **520**:18-24.
37. Wehling-Henricks M, Jordan MC, Roos KP, Deng B, Tidball JG: **Cardiomyopathy in dystrophin-deficient hearts is prevented by expression of a neuronal nitric oxide synthase transgene in the myocardium.** *Hum Mol Genet* 2005, **14**:1921-1933.

Pre-publication history

The pre-publication history for this paper can be accessed here:

http://www.biomedcentral.com/1471-2261/6/47/prepub

Available online at www.sciencedirect.com
SCIENCE DIRECT
ELSEVIER
Biochemical and Biophysical Research Communications 341 (2006) 864–873
BBRC
www.elsevier.com/locate/ybbrc

Functional heterogeneity of side population cells in skeletal muscle

Akiyoshi Uezumi, Koichi Ojima, So-ichiro Fukada, Madoka Ikemoto, Satoru Masuda, Yuko Miyagoe-Suzuki, Shin'ichi Takeda *

Department of Molecular Therapy, National Institute of Neuroscience, National Center of Neurology and Psychiatry, 4-1-1 Ogawa-higashi, Kodaira, Tokyo 187-8502, Japan

Received 18 December 2005
Available online 23 January 2006

Abstract

Skeletal muscle regeneration has been exclusively attributed to myogenic precursors, satellite cells. A stem cell-rich fraction referred to as side population (SP) cells also resides in skeletal muscle, but its roles in muscle regeneration remain unclear. We found that muscle SP cells could be subdivided into three sub-fractions using CD31 and CD45 markers. The majority of SP cells in normal non-regenerating muscle expressed CD31 and had endothelial characteristics. However, $CD31^-CD45^-$ SP cells, which are a minor subpopulation in normal muscle, actively proliferated upon muscle injury and expressed not only several regulatory genes for muscle regeneration but also some mesenchymal lineage markers. $CD31^-CD45^-$ SP cells showed the greatest myogenic potential among three SP sub-fractions, but indeed revealed mesenchymal potentials in vitro. These SP cells preferentially differentiated into myofibers after intramuscular transplantation in vivo. Our results revealed the heterogeneity of muscle SP cells and suggest that $CD31^-CD45^-$ SP cells participate in muscle regeneration.

Keywords: Side population cells; Muscle regeneration; Mesenchymal differentiation; Transplantation

Adult skeletal muscles have a remarkable ability to regenerate following muscle damage. This regeneration has been attributed to satellite cells that reside between the sarcolemma and the basal lamina. Satellite cells are quiescent mononucleated cells in normal conditions, however, in response to muscle damage, they become activated, proliferate, and then exit the cell cycle either to renew the quiescent satellite cell pool or to differentiate into mature myofibers. Thus, they have been considered to be the myogenic precursor cells that give rise to myoblasts and the sole source of adult myogenic cells [1].

In 1998, Ferrari et al. [2] have demonstrated for the first time that bone marrow (BM)-derived cells contribute to the skeletal muscle after BM transplantation. Side population (SP) cells were first identified in bone marrow based on the ability to exclude Hoechst 33342 dye as an enriched fraction of hematopoietic stem cells (HSCs) [3], later, it has been reported that they also participate in muscle regeneration [4]. Studies using whole BM cells showed that BM-derived mononucleated cells display several characteristics of satellite cells, suggesting that donor-derived BM cells contribute to muscle fibers in a stepwise biological progression [5,6]. However, using single HSC transplantation experiment, Camargo et al. [7] suggested that cells committed to the myeloid lineage contribute to muscle through fusion event. Therefore, multiple mechanisms underlay contribution of BM-derived cells to skeletal muscle regeneration.

SP cells have been also identified in skeletal muscle [4]. Muscle SP cells cannot only reconstitute the hematopoietic system of lethally irradiated mice [4,8], but also differentiate into skeletal muscle cells [4,9]. Furthermore, they have been reported to participate in vascular regeneration [10]. Several lines of evidence suggest that muscle SP cells are a cell population distinct from satellite cells [9,11–13]. While muscle SP cells possess these attractive

* Corresponding author. Fax: +81 42 346 1750.
E-mail address: takeda@ncnp.go.jp (S. Takeda).

0006-291X/$ - see front matter © 2006 Elsevier Inc. All rights reserved.
doi:10.1016/j.bbrc.2006.01.037

features, they have been reported to be heterogeneous population. In fact, muscle SP cells contain both $CD45^+$ and $CD45^-$ cells, and hematopoietic potential has been exclusively found in $CD45^+$ fraction [8,9]. As regards the myogenic potential, both $CD45^+$ and $CD45^-$ fractions have been shown to differentiate into skeletal muscle cells [9,14], but there is no comparative study dealing with subpopulation of muscle SP cells during muscle regeneration.

In the present study, we have further divided muscle SP cells into three sub-fractions using CD31 and CD45, examined the properties of each sub-fraction, and identified a novel subpopulation ($CD31^-CD45^-$ SP cells) that showed the greatest myogenic potential both in vitro and in vivo. These results provide a new insight for stem cell-based therapy of muscular dystrophy.

Materials and methods

Animals. All procedures using experimental animals were approved by the Experimental Animal Care and Use Committee at the National Institute of Neuroscience. Eight- to ten-week-old C57BL/6 mice were purchased from Nihon CLEA (Japan). GFP Tg mice were provided by Dr. M. Okabe (Osaka University) and used in cell transplantation experiments. NOD/*scid* mice provided by the Institute for Experimental Animals, Japan, were used as recipients.

To induce muscle regeneration, 100 μl of CTX (10 μM in saline, Wako Chemicals) was injected into the tibialis anterior (TA) muscle with a 29-gauge needle. In FACS analysis experiments, CTX was injected into TA (50 μl), gastrocnemius (50 μl), and quadriceps femoris muscles (25 μl).

BM transplantation was performed as previously described [14]. Mice were subjected to analysis 12 weeks after transplantation.

Antibodies. Mouse Bcrp-1 cDNA was provided by Dr. A.H. Schinkel [15]. A DNA fragment corresponding to cytoplasmic domain of Bcrp1, amino acids 300–337, was fused to GST in a pGEX-4T-2 vector (Amersham Biosciences), and the fusion protein was used to immunize rabbits. The serum obtained was affinity-purified. Other antibodies used in these studies are listed in Table S1.

Cell preparation and FACS analysis. Muscle-derived mononucleated cells were prepared from C57BL/6 mice, GFP Tg mice, or GFP-BM transplanted mice as previously described [14]. Hoechst staining was performed as described by Goodell et al. (http//www.bcm.tmc.edu/genetherapy/goodell/new_site/protocols.html). Cells were re-suspended at 10^6 cells per ml in DMEM (Invitrogen) containing 2% FBS (Trace Biosciences), 10 mM Hepes, and 5 μg/ml Hoechst 33342 (Sigma), and incubated for 90 min at 37 °C in the presence or the absence of 50 μM verapamil (Sigma). During incubation, cells were mixed 3–4 times. For analysis of Ac-LDL uptake, 10 μg/ml DiI-labeled Ac-LDL (Biomedical Technologies) was added. After antibody staining, cells were re-suspended in PBS containing 2.5% FBS and 2 μg/ml propidium iodide (PI) (BD PharMingen). Cell sorting was performed on a FACS VantageSE flow cytometer (BD Biosciences). Debris and dead cells were excluded by forward scatter, side scatter, and PI gating. Cell viability after staining and sorting was comparable to that previously reported [14].

RNA extraction and RT-PCR. Total RNA was extracted from 1×10^4 FACS sorted cells by using a RNeasy Micro Kit (Qiagen) and then reverse transcribed into cDNA by using TaqMan Reverse Transcription Reagents (Roche). The PCRs were performed with 1 μl cDNA product under the following cycling conditions: 94 °C for 3 min followed by 40 cycles of amplification (94 °C for 15 s, 60 °C for 30 s, and 72 °C for 30 s) with a final incubation at 72 °C for 5 min. Specific primer sequences used for PCR are available on request.

Cell culture. SP cells were cultured alone with growth medium (GM); DMEM containing 20% FBS and 2.5 ng/ml bFGF (Invitrogen) in chamber slides (Nalge Nunc) coated with Matrigel (BD Biosciences) for 3–5 days. For osteogenic differentiation, the medium was changed to a differentiation medium (DM), 5% horse serum in DMEM supplemented with or without 500 ng/ml recombinant human BMP2 (R&D Systems), and cultured for 4–6 days. For adipogenic differentiation, cells were exposed to 3 cycles of 3 days of adipogenic induction medium (Cambrex Bioscience) followed by 1 day of adipogenic maintenance medium (Cambrex Bioscience) and then cells were maintained for five more days in the adipogenic maintenance medium. Alkaline phosphatase (AP) was stained using Sigma kit #85 according to the manufacturer's instructions. To stain lipids, cells were fixed in 10% formalin, rinsed in water and then 60% isopropanol, stained with Oil red O in 60% isopropanol, and rinsed in water. For myogenic differentiation, muSP-31, muSP-45, or muSP-DN purified from GFP Tg mice were co-cultured with myoblasts prepared from C57BL/6 mice as previously described [16,17] in GM. DM was supplied 3–5 days after starting co-culture.

Osteogenic activity and myotube-forming activity were determined by the following formulas: osteogenic activity = [the number of AP^+ cells in seven randomly selected fields (corresponding to one-tenth of the whole area of the well)]/(the number of seeded cells) and myotube-forming activity = (the number of GFP^+ myotubes in seven randomly selected fields)/(the number of seeded cells). In order to measure the extent of adipogenic differentiation, stained oil droplets were extracted for 5 min with 100 μl of 4% Nonidet P-40 in isopropanol, and the absorbance of the dye-triglyceride complex was measured at 520 nm [18]; then, adipogenic activity was determined by the following formula: (the absorbance at 520 nm)/(the number of seeded cells).

Intramuscular transplantation experiments. muSP-DN or muSP-31 cells were purified from GFP Tg mice and were injected directly into the TA muscles of NOD/*scid* mice. One day before transplantation, host TA muscles were treated with CTX. The number of transplanted cells is indicated in Table 1. Three weeks after transplantation, TA muscles were excised and fixed in 4% PFA for 30 min, immersed sequentially in 10% sucrose/PBS and 20% sucrose/PBS, and frozen in isopentane cooled with liquid nitrogen.

Immunohistochemistry. FACS sorted cells were collected by Cytospin3 (ThermoShandon). Cells were fixed with 4% PFA for 5 min. Frozen muscle tissues were sectioned using a cryostat. Specimens were blocked with 5% goat serum (Cedarlane) in PBS for 15 min and incubated with primary antibodies at 4 °C overnight, followed by secondary staining. Stained cells were mounted in Vectashield with DAPI (Vector) and photographed using a fluorescence microscope IX70 (OLYMPUS) equipped with a QuantixTM air-cooled CCD camera (Photometrics) and IP Lab software (Scanalytics Inc.). Stained muscle sections were counterstained with TOTO-3 (1:5000; Molecular Probes), then mounted in Vectashield (Vector), and observed under the confocal laser scanning microscope system TCSSP (Leica).

Statistics. Values were expressed as means ± SD or ± SEM. Statistical significance was assessed by Student's *t* test. In comparison of more than two groups, one-way analysis of variance (ANOVA) followed by the Fisher's PLSD was used. A probability of less than 5% ($P < 0.05$) or 1% ($P < 0.01$) was considered statistically significant.

Table 1
Appearance of GFP^+ myofibers after intramuscular transplantation

Cell type	Experiment No.	Number of injected cells/TA muscle	Number of GFP^+ myofibers/TA muscle
muSP-DN cells	Ex. 1	1.7×10^3	14
	Ex. 2	2.5×10^3	9
	Ex. 3	2.5×10^3	0
muSP-31 cells	Ex. 1	1.6×10^4	3
	Ex. 2	1.6×10^4	0
	Ex. 3	1.6×10^4	0

Results

Most muscle SP cells are found in a subset of capillary or vein endothelial cells in non-regenerating skeletal muscle

We identified verapamil-sensitive SP cells in skeletal muscle after Hoechst staining (Fig. 1A) and analyzed the expression of several markers on them. The majority of muscle SP cells were $CD31^+$, usually recognized as a marker of endothelial cells (Figs. 1B–E), and negative for a pan-hematopoietic marker, CD45 (Fig. 1B). More than half of muscle SP cells were $CD34^+$, and $Sca\text{-}1^+$ cells comprised 90% of muscle SP cells (Figs. 1C and D). Compared to FACS profiles of whole-muscle-derived cells, SP cells were enriched in $Sca\text{-}1^+$ cells (Fig. S1). More than 85% of muscle SP cells were $CD31^+$ and took up acetylated low-density lipoprotein (Ac-LDL), a functional marker for endothelial cells and macrophages (Fig. 1E). These results indicate that most muscle SP cells have endothelial characteristics. Only cells in the main population (MP) were found to be $Pax7^+$, indicating that SP cells do not include muscle satellite cells (data not shown).

To examine the localization of muscle SP cells, we generated a rabbit polyclonal anti-mouse Bcrp1 antibody, because it has been reported that Bcrp1 is the major determinant of the SP phenotype [19]. Our antibody clearly recognized Bcrp1 expression in liver, small intestine, and kidney, as previously reported (Fig. S2) [20,21]. We confirmed that Bcrp1 antibody recognizes more than 80% of SP cells and less than 3% of MP cells collected by cytospin (Figs. 1F and G). In skeletal muscle, $Bcrp1^+$ cells were found outside the muscle basal lamina (Fig. 1H), which clearly distinguished $Bcrp1^+$ cells from satellite cells. Next, Bcrp1 expression in the vascular system was investigated. CD31 staining identified all endothelia from larger vessels to capillaries in muscle sections. Intriguingly, Bcrp1 was expressed by CD31-expressing endothelial cells, and its expression was preferentially observed on a subpopulation of capillary endothelium (Figs. 1I–K) and venous endothelium surrounded by thin vessel walls, as revealed by α-smooth muscle actin (αSMA) expression (Figs. 1L–N). These results, together with the results of FACS analysis, strongly suggest that the majority of muscle SP cells are a subset of endothelial cells present in capillaries or veins in non-regenerating skeletal muscle.

Behavior of muscle SP cells during muscle regeneration

We next examined the kinetics of SP cells during muscle regeneration induced by injection of cardiotoxin (CTX). After CTX injection, the total number of mononuclear cells per muscle weight gradually increased, with a peak at day 3. The number of SP cells also increased and reached its peak at day 3 (Fig. 2A). Muscle SP cells could be divided into three subpopulations based on CD31 and CD45 expression: $CD31^+CD45^-$ SP cells (designated muSP-31 cells), $CD31^-CD45^+$ SP cells (muSP-45 cells), and $CD31^-CD45^-$ SP cells (muSP-DN cells). muSP-31 cells and muSP-DN cells distributed throughout the SP tail, but muSP-45 cells were located close to the shoulder (data not shown). The majority of muscle SP cells in untreated muscle were muSP-31 cells (Fig. 1B). During regeneration, however, muSP-45 cells and muSP-DN cells increased in both their ratios and their numbers (Figs. 2B and C). Although $CD45^+$ cells were abundant in whole muscle-derived cells during regeneration and most of them were F4/80 antigen-positive mature macrophages, SP cells did not contain any mature inflammatory cells, as previously reported (data not shown) [14].

To clarify the origin of each subpopulation of SP cells, BM transplantation experiments were performed. We confirmed that muSP-45 cells were mobilized from bone marrow as previously reported (Figs. 3A and B) [14]. In contrast, both $CD45^-$ SP fractions are residents of skeletal muscle (Figs. 3A and B), consistent with the results reported by Rivier et al. [22].

Next, to determine whether each subpopulation of SP cells proliferates in damaged muscle, cells were stained with Ki67 antibody. Most muSP-45 cells (Figs. 3C and D) and muSP-31 cells (Figs. 3G and H) prepared from regenerating muscle were negative for Ki67, suggesting that the proliferation activities of these two fractions were low. On the other hand, about 60% of muSP-DN cells were positive for Ki67 (Figs. 3E and F), indicating that muSP-DN cells actively proliferated during muscle regeneration.

We next examined Bcrp1 expression on three sub-fractionated SP cells and found that only muSP-31 cells were Bcrp1-positive (Fig. 3K). These results suggest that some ABC transporters other than Bcrp1 are responsible for the phenotype of $CD31^-$ SP cells.

Gene expression of muscle SP cells during muscle regeneration

Our analysis revealed that each subpopulation of SP cells showed distinct kinetics during muscle regeneration. To better understand the traits of muscle SP cells, we analyzed gene expression during muscle regeneration. Three subpopulations of SP cells (in following experiments, muSP-45 cells from untreated muscle were omitted because of their low yield) or MP cells were collected from each time point during muscle regeneration, and RT-PCR was performed. We chose several myogenic (*Pax3*, *Pax7*, and *myf5*), endothelial (*Tie2*, *Flk1*, and *vWF*), and mesodermal-mesenchymal-associated (*αSMA*, *PPARγ*, *Runx2*, *PDGFRα*, and *PDGFRβ*) genes to clarify lineage characteristics of the target cells. We also examined expression of genes of developmental regulators (*msx1*, *Frizzled4* (*Fzd4*), *Patched1* (*Ptc1*), and *BMPR1A*), angiogenic factors (*angiopoietin-1* (*ang1*) and *VEGF*), and TGF-β superfamily antagonists (*follistatin* and *DAN*). muSP-DN cells from untreated muscles expressed only *PDGFRβ*, *Ptc1*, *ang1*, *follistatin*, and *DAN* (Fig. 4, cont, lane 1). Neither myogenic nor other lineage-specific markers could be detected in

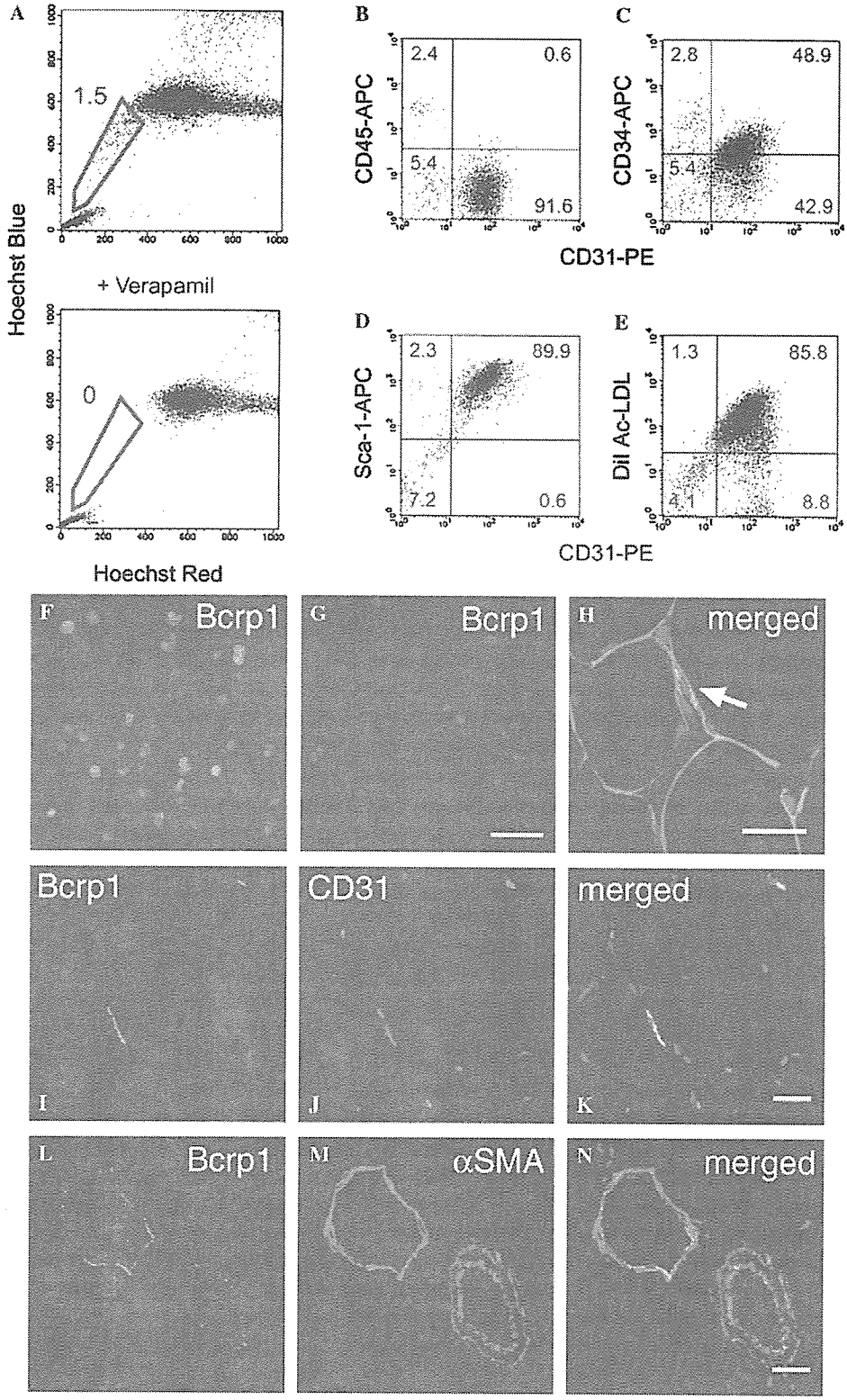

Fig. 1. Characterization of skeletal muscle SP cells. (A) Flow cytometric analysis of muscle-derived mononucleated cells after Hoechst 33342 staining with (lower panel) or without Verapamil (upper panel). The numbers indicate the percentage of SP cells (blue pentagons) in all mononucleated cells. (B–E) The expression of CD45 (B), CD34 (C), Sca-1 (D), and DiI-Ac-LDL uptake (E), and CD31 (B–E) on muscle SP cells. The percentage of cells in each quadrant is shown in the panel. (F,G) Immunofluorescent staining for Bcrp1 (green) and DAPI counterstaining (blue) of freshly sorted SP (F) and MP (G) cells. Immunofluorescent staining for Bcrp1 (green) and laminin α2 chain (red) (H), Bcrp1 (green) and CD31 (red) (I–K), and Bcrp1 (green) and α-smooth muscle actin (red) (L–N). TOTO-3 nuclear staining is shown in merged images (blue in H, K, and N). Bcrp1-positive cells are located outside the basal lamina (arrow), and they are partially overlapped with endothelial cells of capillary (I–K) and vein (L–N). Bars: 50 μm in (F,G), 20 μm in (H–N).

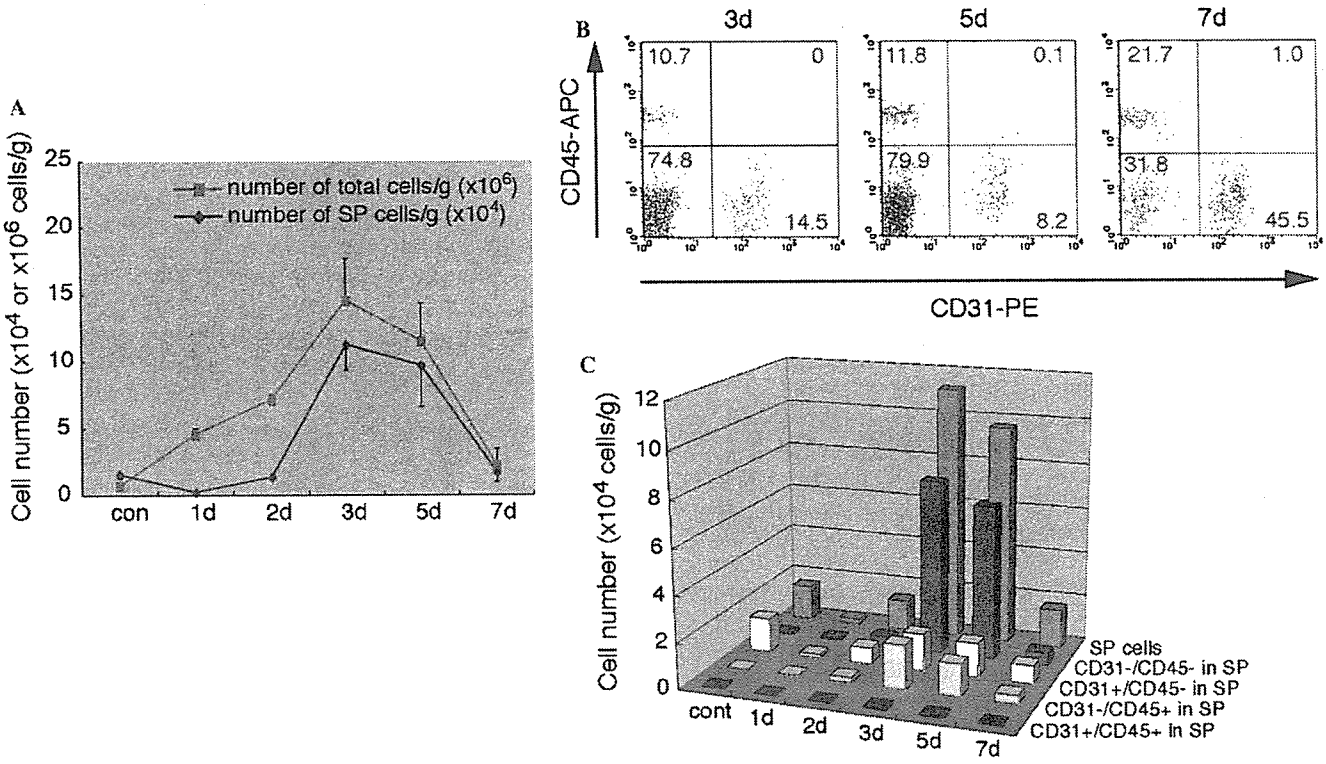

Fig. 2. Behavior of subpopulations of SP cells during muscle regeneration. (A) At 1 day (1d), 2 days (2d), 3 days (3d), 5 days (5d), and 7 days (7d) after CTX injection, the number of total cells (pink line) and SP cells (blue line) per gram of muscle weight was quantified. (B) At 3 days (3d), 5 days (5d), and 7 days (7d) after CTX injection, muscle SP cells prepared from regenerating muscle were analyzed for CD31 and CD45 expression. (C) Cell numbers in subpopulations of SP cells. muSP-45 cells (light blue bar) and muSP-DN cells (dark red bar) were significantly increased in number during muscle regeneration. Values (A,C) are the average of three independent experiments. Error bars represent SD.

this population indicating that muSP-DN cells do not contain cells committed to the lineages tested. At day 3 after CTX injection, muSP-DN cells began to express developmental regulator genes (Fig. 4, 3d, lane 1), and then at day 5, they also began to express several other lineage-specific genes (*Tie2*, *αSMA*, *PPARγ*, and *Runx2*). Angiogenic factors and TGF-β superfamily antagonists were also strongly expressed at this time point (Fig. 4, 5d, lane 1). In contrast, muSP-31 cells continuously expressed all three endothelial genes analyzed throughout the regeneration process (Fig. 4, lane 2). Expression of mature endothelial marker, such as *vWF*, suggests that muSP-31 cells represent committed endothelial cells. muSP-45 cells expressed only low levels of *αSMA*, *PDGFRβ*, and *follistatin* at day 5 after CTX injection (Fig. 4, lane 3). Myogenic markers, *Pax7* and *myf5*, were detected only in the MP fraction (Fig. 4, MP) indicating that myogenic cells are completely sorted into the MP fraction even during the process of muscle regeneration.

Differentiation potential of muscle SP cells for mesenchymal lineages

muSP-DN cells showed a unique gene expression pattern during muscle regeneration process: they began to express several mesenchymal genes at a late phase of muscle regeneration. Therefore, we examined the mesenchymal potentials of muscle SP subpopulations. muSP-DN cells from untreated muscle readily gave rise to alkaline phosphatase (AP)-positive cells when cultured in the presence of bone morphogenetic protein 2 (BMP2) (Figs. 5A and C). With adipogenic induction, they also differentiated into adipocytes containing numerous lipid droplets in the cytoplasm (Figs. 5A and D). Reflecting the results of gene expression analysis, muSP-DN cells from regenerating muscle more efficiently differentiated into osteogenic cells and adipocytes than those from untreated muscle did (Figs. 5B–D). Unexpectedly, muSP-DN cells from regenerating muscle also differentiated into adipocytes without adipogenic induction (Figs. 5B and D), suggesting that they are susceptible to adipogenesis under our culture condition. In contrast, muSP-31 cells did not possess these differentiation potentials (Figs. 5A–D). Nor did muSP-45 cells, which were dramatically mobilized from BM into regenerating muscle (Figs. 5B–D). The attribute of differentiation potential is therefore a feature of muSP-DN.

Myogenic potential of muscle SP cells in vitro

We next evaluated the myogenic potential of muscle SP cells in vitro. When SP cells were cultured alone, they never differentiated into skeletal muscle cells (data not shown). Each subpopulation of SP cells was prepared from GFP Tg mice and co-cultured with wild type (WT) primary

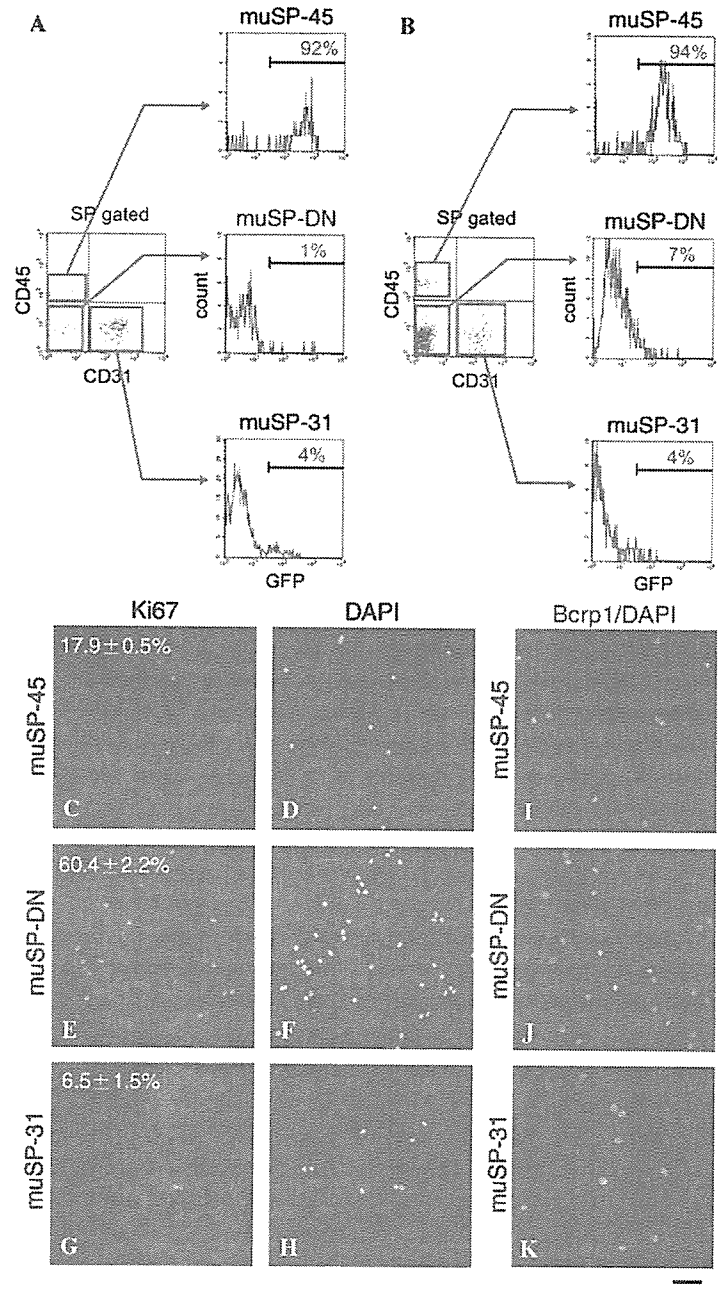

Fig. 3. Origin, proliferative activity, and Bcrp1 expression of subpopulations of muscle SP cells. (A,B) C57BL/6 mice were transplanted with whole BM from GFP Tg mice, and 3 months later, SP cells from untreated muscle (A) or regenerating muscle (3 days after CTX injection) (B) were further analyzed for CD31, CD45, and GFP expression. Note that $CD45^-$ SP cells (middle and lower panels) are almost all negative for GFP, indicating that they do not originate from BM. In contrast, more than 90% of muSP-45 cells were GFP^+ (upper panels). (C–H) Ki67 expression (green) and nuclei stained with DAPI (blue) on muSP-45 (C,D), muSP-DN (E,F), and muSP-31 (G,H) cells. The percentages of Ki67-positive cells were expressed as means ± SD of three independent experiments. muSP-45 (I), muSP-DN (J), and muSP-31 (K) were sorted from regenerating muscle and stained for Bcrp1 (green) and nuclei (blue). Only muSP-31 cells were stained positive for Bcrp1 (K). Bar: 50 μm.

myoblasts derived from satellite cells. muSP-DN cells from untreated muscle rapidly proliferated in vitro as observed in regenerating muscle (Fig. 2C). On the contrary, muSP-31 cells hardly expanded. After 2–3 weeks co-culture, both muSP-DN cells and muSP-31 cells differentiated not only into multinucleated myotubes co-expressing GFP and sarcomeric-α-actinin (Figs. 5E–G, only muSP-DN culture is shown) but also mononucleated myocytes (shown in insets). The frequency of mononucleated myocytes was too low to quantify, but existence of these cells suggests that myogenic differentiation of SP cells could occur without fusion. Strikingly, the myotube-forming activity (the frequency of GFP^+ myotubes, see Materials and methods for details) of muSP-DN cells was approximately 10-fold that of muSP-31 cells (Fig. 5H, lane for cont, 0.026 ± 0.007 vs 0.002 ± 0.001). In the experiments using SP cells from regenerating muscle at 3 days after CTX injection, muSP-DN cells showed the highest

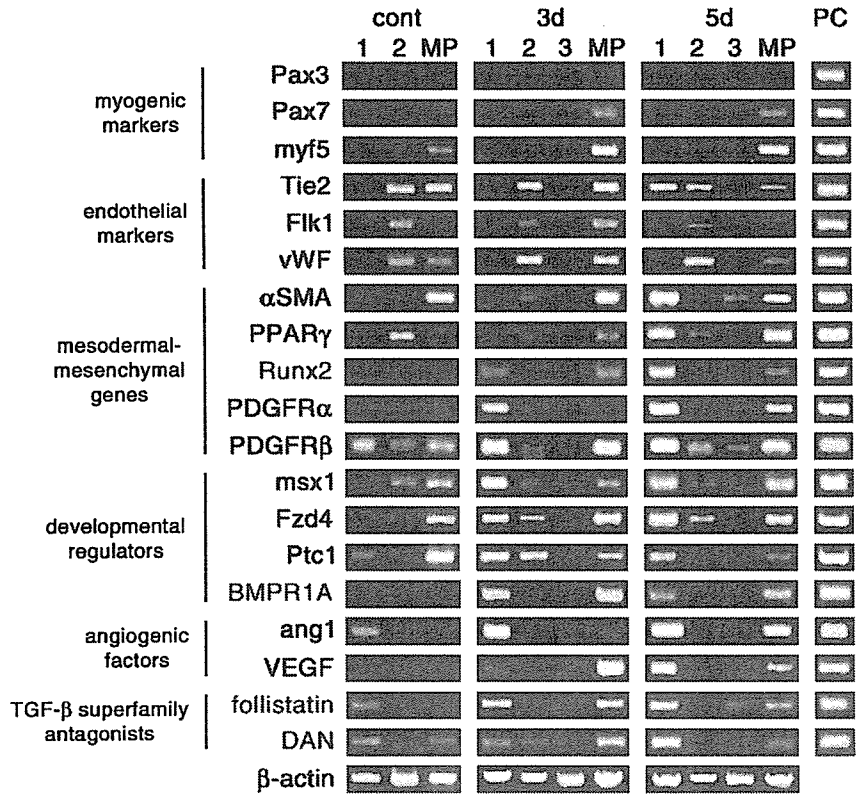

Fig. 4. Gene expression profiles of muscle SP cells during muscle regeneration. muSP-DN (lane 1), muSP-31 (lane 2), muSP-45 (lane 3), or MP cells were collected from untreated (cont) and regenerating muscle at 3 days (3d) or 5 days (5d) after CTX injection, and RT-PCR was performed against the indicated genes. Total embryo extract (E13) was used as a positive control (PC). β-actin was amplified to confirm that the quantities of mRNA were equal.

myotube-forming activity, although each SP subpopulation did form myotubes co-expressing GFP and sarcomeric-α-actinin (Fig. 5H, lane for CTX3d). This clearly demonstrates that muSP-DN cells have the highest myogenic potential among SP sub-fractions in vitro. For comparison, we quantified the myotube-forming activity of satellite cell-derived myoblasts. The value was 0.09 ± 0.01, indicating that myogenic activity of myoblasts is much higher than that of muSP-DN cells.

Myogenic potential of muscle SP cells in vivo

To evaluate the myogenic potential of muscle SP cells in vivo, we performed transplantation experiments. muSP-DN or muSP-31 cells from untreated muscle of GFP Tg mice were directly transplanted into CTX-treated TA muscles of immunodeficient NOD/*scid* mice. Three weeks after transplantation, muSP-DN cells had generated myofibers more efficiently than muSP-31 cells (Figs. 6A and B, and Table 1), indicating that muSP-DN cells had relatively higher myogenic potential in vivo as well as in vitro. Contrary to our expectation, muSP-DN cells formed no GFP-positive adipocytes after transplantation.

Discussion

Muscle SP cells have been suggested to be multipotent and can contribute to skeletal muscle regeneration [4,9,10,23]. However, most of these studies dealt with whole muscle SP cells as one functional unit. We subdivided, for the first time, muscle SP cells using CD31 and CD45 markers and revealed functional heterogeneity of muscle SP cells. $CD31^+CD45^-$ SP cells (muSP-31 cells) are a main subpopulation in non-regenerating muscle, but $CD31^-CD45^-$ SP cells (muSP-DN cells) which represent a minor subpopulation in non-regenerating muscle have the greatest differentiation potentials and become predominant subpopulation of SP cells upon muscle injury.

Differentiation potential of muscle SP cells

Phenotypic and immunohistochemical analysis suggested that muSP-31 cells are a subset of endothelial cells of capillaries and veins. They poorly proliferate after injury or in in vitro culture, and their differentiation potentials are limited both in vitro and in vivo.

$CD45^+$ muscle SP cells (muSP-45 cells) were shown to have both hematopoietic and myogenic potentials, and hematopoietic potential of muscle-derived cells was exclusively found in this fraction [8,9]. We previously reported the contribution of muSP-45 cells to muscle regeneration [14]. In this study, we identified novel subpopulation that possesses much higher myogenic potential than muSP-45, muSP-DN.

muSP-DN cells showed the highest differentiation potential of all the mesenchymal lineages tested among

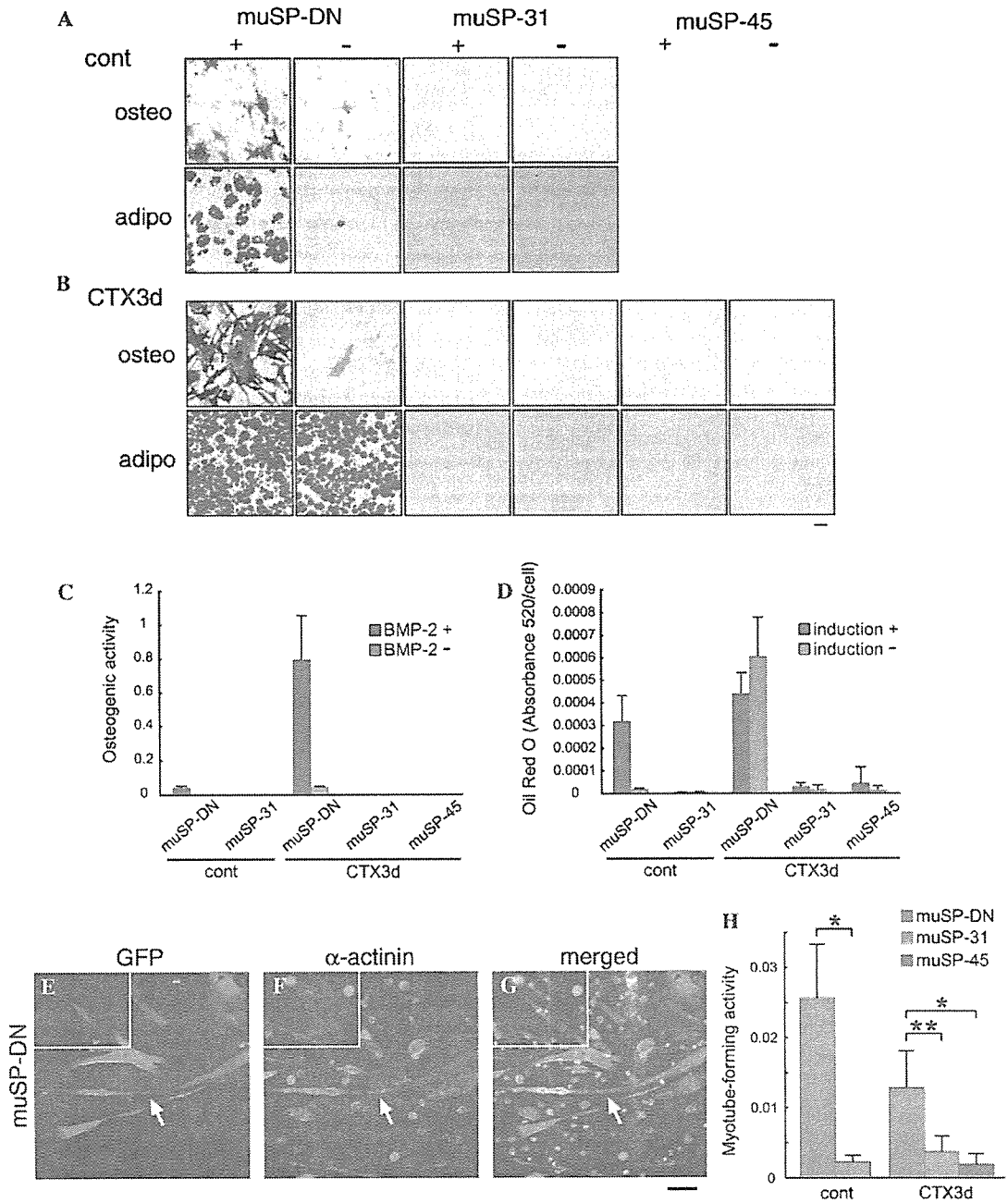

Fig. 5. muSP-DN cells differentiate into osteogenic cells, adipocytes, and skeletal muscle cells. (A,B) Three subpopulations of SP cells prepared from untreated (A) or regenerating (B) muscle were induced to differentiate into osteogenic or adipogenic cells. Uninduced cells (−) and induced cells (+) were then examined for alkaline phosphatase expression (osteo) or oil deposits (adipo). Bar: 50 μm. (C,D) Osteogenic (C) and adipogenic (D) activities of subsets of SP cells prepared from control (cont) or regenerating muscle at 3 days after CTX injection (CTX3d) were quantified. Values are the average of three independent experiments. Error bars represent SD. (E–G) Co-culture of muscle SP cells with myoblasts. muSP-DN cells from GFP Tg mice were sorted and co-cultured with WT primary myoblasts in differentiation medium. Cells were stained with anti-GFP (green) and anti-sarcomeric α-actinin (red) antibodies. Nuclear staining with DAPI (blue) is shown in merged images (G). Insets show GFP^+ mononucleated myocyte. Bar: 50 μm. (H) Myotube-forming activities of muSP-DN cells (red bars), muSP-31 cells (blue bars), and muSP-45 cells (green bar) are shown. Each subpopulation was prepared from untreated (cont) or CTX-treated regenerating muscle (CTX3d). Values are the average of three independent experiments. Error bars represent SD. $^*P < 0.01$, $^{**}P < 0.05$.

SP subpopulations. They were negative for lineage-specific markers under the non-regenerating condition, but after muscle injury or in in vitro expansion, they actively proliferated and were readily induced to express several mesenchymal genes. Their differentiation potential seems to be restricted to mesenchymal lineages because we did not detect hematopoietic colonies derived from muSP-DN cells in vitro and muSP-DN cells failed to rescue the lethally irradiated mice (data not shown). These observations indicate that muSP-DN cells are enriched for primitive mesenchymal cells. This notion is further supported by gene expression pattern of muSP-DN cells. muSP-DN cells